Science of Sintering, **49** (2017) 247-261

doi: https://doi.org/10.2298/SOS1703247R

UDK 678.046.3, 612.086.3, 620.181.4

The Chemometric Study of Limestone Physico-chemical Properties and Thermal Behavior for Application in Construction Composites

Dragan Radulović[1], Anja Terzić[2*)], Lato Pezo[3], Ljubiša Andrić[1], Irena Grigorova[4]

[1]Institute for Technology of Nuclear and other Mineral Raw Materials, Franchet d'Esperey 86, 11000 Belgrade, Serbia

[2]Institute for Testing of Materials IMS, Vojvode Mišića Bl. 43, 11000 Belgrade, Serbia

[3]Institute of General and Physical Chemistry, University of Belgrade, Studentski Trg 12-16,11000 Belgrade, Serbia

[4]University of Mining and Geology "St. Ivan Rilski", Department of Mineral Processing and Recycling, 1700 Sofia, Bulgaria

Abstract:

The limestone, as an economically sustainable and easily available basic raw material, is frequently utilized in the building industry for resolving of the environmental protection issues. The limestone is incorporated in a cementitious system either by grinding with cement clinker, or by blending with the binder during concrete production. The employing of powdery limestone as partial cement replacement gives the construction composites with properties comparable to that of conventional concrete. The study of limestone thermal behavior and its chemistry is crucial for the prognosis of the designed composites properties. In this work, the instrumental techniques (atomic emission spectroscopy, differential thermal and thermo-gravimetric analysis, Fourier transform infrared spectroscopy) and the Principal component analysis were employed to discriminate and classify 22 limestone types. The PCA statistical method, as a means of spectra and experimental data fingerprinting, grouped the samples in a multi-dimensional factor space producing four graphical prognosis - one for each instrumental method. DTA/TG peak values varied the most in a short range between 830-870 ℃, while FTIR spectra showed the highest diversity in the 867-887 cm^{-1} and 1237-1647 cm^{-1} ranges. This research was governed by an idea to reveal whether it is possible to differentiate various limestone types and to predict the possibility of their employment in construction composites on the basis of the results of instrumental and mathematical analyses.

Keywords: *Thermal behavior; Chemical analysis; Microstructure; FTIR; DTA/TG; SEM; Binder; Filler.*

1. Introduction

The limestone is a sedimentary rock predominantly comprising carbonate minerals (i.e. calcium carbonate, $CaCO_3$) in the quantity that surpasses 50 %. Quartz and clay minerals

*) **Corresponding authors:** anja.terzic@institutims.rs

(e.g. kaolinite, hydrous mica, montmorillonite) are other two major constituents of the limestone [1]. Since a substitution of calcium by magnesium occasionally occurs, a limestone that contains 5-35 % of Mg is defined as "magnesian limestone". If Mg content is below 5 %, the rock is classified as a "high-calcium limestone" [2]. The carbonates present in the limestone customarily appear as calcite, aragonite and/or vaterite mineral phases. However, the only crystal form of real significance is calcite [3]. By being the most abundant and enclosing at least 50 % of all present mineral phases in the limestone, calcite is an important resource and subject of investigations in various scientific fields: mineralogy, chemistry, physics, materials science [4-7]. The crystalline structure of calcite is commonly illustrated by the $R\bar{3}c$ trigonal space group [8]. Due to the perfect rhombohedral cleavage, calcite exhibits a small value of Mohs hardness (3.0). The specific gravity of calcite is 2.7 [3]. The thermally induced behavior, i.e. calcium carbonate stability constrains and the rules of phase transitions, represents a basis for a comprehensive study of the limestone [9-11]. Due to the alternations in carbonate mineral phases at different temperatures, materials of diverse compositions can be obtained for use in a variety of applications.

Limestone is an economically sustainable and easily available resource; therefore, both in its crude and powdery form, the limestone can be readily produced and utilized [12]. Natural limestone minerals are the basic raw materials for building industry and for resolving of the environmental protection issues [1]. Namely, the limestone is extensively employed in the interior and exterior as architectural stones and walls, in the production of lime (CaO), as coarse aggregates and fillers in construction composites (concretes and mortars), in paint and polymer fabrication as fillers, as metallurgical flux, in road building (aggregates for highways and runways, railroad ballasts, embankments, soil stabilization agents) [13-15]. Since the limestone is able to decrease the CO_2 footprint of concrete by approximately 15 %, it became one of the base materials used in the manufacturing of Portland cement (PC) and one of the most common mineral additions with low reactivity [12, 16].

The application of powdery limestone as partial cement replacement gives the construction composites with properties comparable to that of conventional concrete [17]. The limestone incorporation in cementitious systems is performed either by limestone grinding with the PC clinker, or supplementary blending of PC with limestone powder during concrete production [18]. The first method results in the composite system with a finer limestone phase, while the second method produces a material with a precisely controlled limestone grain-size distribution. The grinded limestone accelerates hydration reactions, amends the particles packing, induces the carboaluminates formation that decreases the overall pore volume, and finally results in minimized strength loss associated with limestone [18]. The blended limestone influences the cementitous composite through a series of physical and chemical impacts. Used as an additive in the concrete design, the limestone enhances the viscosity, increases the workability and improves the flowability of a green mixture by causing alternations in particle size, heterogeneous nucleation and dilution (reduced coagulation and increased clinker particle dispersion). Also, the inclusion of the limestone is a prerequisite for reduction of the initial and final concrete setting times followed by a minimal increase in total shrinkage in comparison with the conventional concretes [17]. The chemical influence relates to the cement hydration and the reaction of limestone with calcium aluminate to form calcium mono-carboaluminate [19]. The addition of the limestone powder leads to the premature cement hydration and supplies nucleation sites for the C-S-H gel formation. The cementitous composite early-age mechanical properties are enhanced due to the promoting impact that limestone powder has on the cement hydration, while final strengths are reduced because of the dilution effect [12].

The study of the thermal decomposition reactions of limestone minerals and the chemistry of the limestone constituents is relevant for the analysis and prognosis of the properties and behavior of designed construction composites and the assessment of their engineering and industrial application possibilities [2, 19-21]. In this work, differential

thermal analysis (DTA), thermo-gravimetric analysis (TGA) and Fourier transform infrared spectroscopy (FTIR) were employed to characterize and discriminate 22 different limestone types. The chemical characteristics of the examined representative samples were also observed. All three instrumental methods (DTA, TGA and FTIR), as well as the chemical analysis, were combined with the Principal component analysis (PCA) to classify the samples. This research was governed by an idea to reveal whether it is possible to differentiate various limestone types and to predict the possibility of their employment in construction composites on the basis of the results of the conducted instrumental and mathematical analyses.

2. Materials and methods

The limestone samples that were used in this study originate from twenty-two different deposits located on the territories of Republic of Serbia and Montenegro. The investigated ore is classified as a sedimentary calcite rock. The crude limestone samples were collected from each deposit, taking into account the differences in the macroscopic composition of the stone in order to be fully representative. Representative ore samples of 50 kg, obtained from each deposit according to the standard ore sampling campaign [22, 23] were used in the investigation. After the initial rough crushing via primary jaw crusher (KHD Humboldt Wedag; Model 5"x 6") and secondary cone crushing (Denver Roll Crusher; Model 6"x10", size: 10 mesh/1.651 mm), the samples were split and bagged in 5 kg sub-samples. The sub-samples were further pulverized for the laboratory analyses in an agate stone mill (KHD Humboldt Wedag), and subsequently packed in the plastic bags and marked as K1-22.

Tab. I Chemical compositions of the K1-22 limestone samples.

Oxide (%)	K1	K2	K3	K4	K5	K6	K7	K8	K9	K10	K11
CaO	55.00	54.84	55.38	54.75	52.07	55.35	55.03	54.05	54.73	54.93	54.97
MgO	0.73	1.04	0.38	1.4	3.61	0.406	1.08	1.61	0.884	0.996	0.605
Fe_2O_3	0.05	0.03	0.02	0.04	0.04	0.02	0.03	0.05	0.06	0.05	0.05
Al_2O_3	0.02	0.08	0.02	0.02	0.03	0.02	0.02	0.08	0.01	0.005	0.03
SiO_2	0.30	0.40	0.19	0.06	0.19	0.23	0.16	0.18	0.24	0.03	0.23
Na_2O	0.02	0.03	0.043	0.024	0.026	0.021	0.025	0.015	0.06	0.054	0.012
K_2O	0.006	0.009	0.006	0.006	0.006	0.005	0.005	0.029	0.015	0.014	0.064
TiO_2	0.02	0.02	0.02	0.02	0.02	0.02	0.02	0.02	0.02	0.02	0.02
P_2O_5	0.005	0.005	0.005	0.005	0.005	0.005	0.005	0.096	0.023	0.028	0.03
LoI	43.8	43.46	43.93	43.63	43.95	43.92	43.62	44.8	44.28	44.78	43.8
pH	9.26	9.14	9.26	9.07	9.13	9.25	9.28	9.40	9.50	9.45	9.35
Oxide (%)	**K12**	**K13**	**K14**	**K15**	**K16**	**K17**	**K18**	**K19**	**K20**	**K21**	**K22**
CaO	54.96	55.27	54.99	55.3	55.08	55.51	55.41	55.52	55.42	54.97	54.98
MgO	0.682	0.306	0.373	0.323	0.646	0.354	0.382	0.301	0.32	0.616	0.627
Fe_2O_3	0.02	0.03	0.02	0.03	0.02	0.03	0.03	0.03	0.04	0.03	0.04
Al_2O_3	0.02	0.01	0.008	0.009	0.01	0.006	0.003	0.004	0.005	0.01	0.03
SiO_2	0.10	0.10	0.52	0.52	0.10	0.10	0.11	0.16	0.27	0.01	0.11
Na_2O	0.003	0.002	0.002	0.003	0.004	0.003	0.002	0.002	0.001	0.003	0.007
K_2O	0.056	0.051	0.048	0.045	0.06	0.041	0.064	0.051	0.046	0.054	0.069
TiO_2	0.02	0.02	0.02	0.02	0.02	0.02	0.02	0.02	0.02	0.02	0.02
P_2O_5	0.006	0.014	0.014	0.011	0.006	0.005	0.091	0.022	0.031	0.015	0.034
LoI	43.83	43.71	43.59	43.75	43.93	43.94	43.91	43.9	43.85	43.83	43.91
pH	9.20	9.35	9.33	9.56	9.34	9.39	9.33	9.51	9.40	9.59	9.35

The chemical analysis of the limestone samples was performed by atomic emission spectroscopy (AES) on a PinAAcle 900 instrument (Perkin Elmer, USA). The five samples, per each limestone type (K1-22), were acquired by cone & quartering method from a 5 kg sub-sample. Representative samples (100g) were pulverized in a laboratory mill prior to the testing, which was conducted in accordance with the standard methods for chemical analyzing (ASTM C25/C1271/C1301) [24-26] The loss on ignition (LoI) was determined as a weight difference between 20° and 1000 °C. The acquired averaged values of the main oxides are presented in the Table I. The determined pH values for all limestone samples were above 9.0 making them very strong alkaline [27].

2.1. Instrumental analyses

Mineralogical analysis of the limestone samples was conducted by means of the X-ray powder diffraction (XRD) technique. The X-ray powder diffraction patterns were acquired on a Philips PW-1710 automated diffractometer using a Cu tube operated at 40 kV and 30 mA. The instrument was provided with a diffracted beam curved graphite monochromator and a Xe-filled proportional counter. Measurements were conducted at ambient temperature (25 °C). The diffraction data were assembled in the 2θ Bragg angle range from 5 to 70°, counting for 1 s (qualitative identification) at every 0.02° step. The divergence and receiving slits were fixed at 1 and 0.1, respectively.

The thermal behavior was monitored by simultaneous differential thermal analysis (DTA) and thermo-gravimetry (TG) in the temperature range from 20° to 1000 °C. DTA/TG analyses were conveyed in a static air flow by an automatic thermo-analyzing system: STA 409EP (Netzsch, Germany). The limestone samples (100 mg) were loosely packed into an alumina holder and thermally treated under a nitrogen atmosphere at a heating rate of 10 °C/min.

The chemical bonds, distinctive molecular fingerprints, functional groups and covalent bonding information were detected via Fourier Transform Infrared (FTIR) spectroscopy analysis. The FTIR spectra were obtained on a Nicolet IS-50 spectrometer (Thermo Fisher Scientific, USA), recorded in KBr transmission mode in the 4000-400 cm^{-1} range and 32 scans at resolution 4.

The morphology of the samples was characterized by scanning electron microscopy (JEOL JSM–6610LV). The investigated samples were covered with gold using a sputter machine, type BALTEC-SCD-005, for improvement of the conductivity prior to the imaging.

2.2. Statistical analysis

The Principal component analysis (PCA), as the main tool in exploratory data analysis, is applied to classify the limestone samples (K1-22) on the bases of the results acquired via instrumental techniques (AES, DTA, TG, and FTIR). This statistical method has been frequently used for fingerprinting of the spectra and/or experimental and instrumentally obtained data of similar samples. It is a multivariate technique where data are transformed into orthogonal components which are linear combinations of the original variables. TGA and DTA peak values, and FTIR and AES spectra reflections were thoroughly examined to show the possible dissimilarities between obtained samples. PCA is performed by Eigenvalue decomposition of a data correlation matrix [28]. All samples were grouped in a multi-dimensional factor space and four PCA graphics were plotted, according to the results of the TG, DTA, FTIR and the chemical analysis (AES) of the investigated limestone samples. The PCA decomposes the original matrix into several products of multiplication into loading (different samples) and score (TG, DTA, FTIR and AES results) matrices. Different samples subjected to different testing conditions were taken as variables (column of the input matrix), while the results of the TG, DTA, FTIR and AES were regarded as mathematical cases (rows

of the matrix). The analysis, in which the first component has the largest possible variance in the transformation, is used to achieve maximum separation between parameter clusters [29, 30]. This approach, evidencing spatial relationship between processing parameters, enabled discrimination between various samples. Descriptive data analysis, i.e. PCA, was performed via software package STATISTICA 10.0 (StatSoft Inc., Tulsa, OK, USA) [31].

3. Results and discussions

The primary constituent of all investigated limestone samples (K1-22) was calcium carbonate ($CaCO_3$), with its content set at approximately 95 %. The lowest $CaCO_3$ content was detected in K5 sample (92.93 %), while the highest $CaCO_3$ percentage was present in K19 sample (99.09 %). High loss on ignition (LoI) also refers to the presence of calcium carbonate as the main combustible component, but also implies the inclusion of clay minerals in limestone mineralogical conformation. With an average value of 55 %, CaO is the principal chemical compound detected by AES technique (chemical analysis results are provided in Tab. I). The investigated limestone also contained Al_2O_3, SiO_2, MgO, Fe_2O_3, Na_2O, K_2O, TiO_2 and P_2O_5 as minor constituents. The content of each of previously mentioned oxides was below 1 %, except MgO whose portion showed the increased value in the chemical analyses of the samples K2 (1.04 %), K4 (1.40 %), K5 (3.61 %), K7 (1.08 %) and K8 (1.61 %). The Principal component analysis (PCA) of the acquired AES results (major and minor constituents) is illustrated in the Fig. 1.

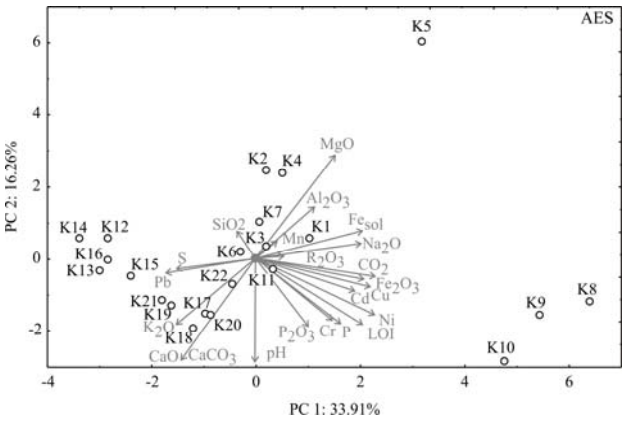

Fig. 1. PCA biplot for the results of the chemical analysis of K1-22 limestone samples.

Since the limestone is identified and utilized as a cement addition and a replacement in PC clinker blends and as a mineral admixture in the design of construction composites (e.g. mortars and concretes), detecting and monitoring its chemical composition is of the uttermost importance. Namely, maintaining the CaO content as high as possible is crucial in order to induce early cement hydration. Thereby, the supplementary nucleation sites for the formation of continuous layer of calciumcarbosilicate hydrates (C-S-H gel) are provided [12]. Their role is to bind together the cement particles into a cohesive composite structure. Additional $CaCO_3$ amount also induces the formation of calcium carboaluminates which are accounted important for the development of construction composites mechanical strengths [32, 33]. The detected CO_2 content in the investigated limestone samples meagerly varied from 43.13 % (K12) to 44.18 % (K8). Keeping the carbon dioxide portion fixed is important for the limestone application in the cement and concrete production where maintaining the CO_2 emission as low as possible in one of the major environmental protection imperatives [34, 35]. The chemical limits regarding the presence of magnesium, sulfur and alkalis (Na, K) are rigorously

regulated for the application of limestone in cement clinker production [36]. The detected quantity of chemical constitutes are always evaluated to assess the feasibility of limestone application in construction composite materials such as concrete and mortar. MgO content is monitored due to the proposed limitation in the cement production standards and because of the risk related to the unsoundness of concrete. The average MgO share that is currently being applied in EU clinker plants is set at 1.05 %, but generally the tolerated maximal MgO content, that does not induce cement deterioration, is between 4.0 % and 6.0 % [36]. The investigated limestone samples are being categorized as high-calcite raw materials, instead of being dolomite rich, therefore the elevated MgO content is detected only in the three samples: K4, K5 and K8. Also an additional limitation has to be set for the MgO and Fe_2O_3 ratio because both oxides behave as fluxes. This ratio (the ratio in the cement clinker should not surpass 1.4 [36]) reduces the possibility of melting and the formation of the defects in the produced material. The Fe_2O_3 content in all samples is below 0.1 % and sulfur content is minor (approximately 0.01 %). The concentrations of trace elements, which belong to four categories depending on their origin and pattern of distribution [37], are also limited. Namely, the average content of Cd, Cr, Cu, Mn, Ni, Pb, and Sb that is tolerated in a limestone-cement composition is: 0.6, 36, 32, 706, 36, 34, and 4 ppm, respectively [36, 37]. The detected maximal concentrations of trace elements in the K1-22 limestone samples were: Cd = 0.55 ppm; Cr = 10 ppm; Cu = 29 ppm, Mn = 35 ppm, Ni = 24 ppm, Pb = 25 ppm, and Sb = 2.5 ppm. All obtained maximal values are lower than appropriate average concentrations reported for the limestone-cement.

As it is illustrated via PCA biplot for the results of AES analysis in Fig. 1, the first principal component (PC1) explained 33.91 % of the total variance, i.e. the first Eigenvalue equals 7.45. The second principal component (PC2) explained 16.26% of the total variance, i.e. Eigenvalue equals 3.50. The maximum of Fe_2O_3, Cu, Cd, Ni, Cr, P, Cr, CO_2, P, P_2O_3 and LoI were observed for samples K8-10 which are located in the right lower corner of the diagram. Therefore, the samples K8-10 are prone to the formation of solid solutions during exposure to elevated temperatures due to high Fe_2O_3 content. The K5 sample is located in the upper right corner of the diagram, and it has the maximal MgO content which is related to presence of dolomite in its mineralogical composition. The K5 has been previously marked as the sample with the lowest $CaCO_3$ content. High Al_2O_3 and Na_2O contents were found in the samples K1-4 and K7 (all positioned on the right side of the graph). High SiO_2, Pb and S percentages were found in the samples K6 and K12-16 (situated on the upper left side of the graph), while the maximal K_2O, CaO and $CaCO_3$ contents were noticed in the samples K17-22 (lower left side of the graph). The provided chemical and PCA analyses indicated the K19 sample as the optimal limestone due to the high $CaCO_3$ content and low percentage of Fe_2O_3 and MgO.

The X-ray powder diffraction patterns of K5 and K19 limestone, as the samples with the most diverse chemical compositions, were obtained and compared in the Fig. 2 (a and b).

The XRD diagrams indicate that the investigated limestone samples are mainly composed of calcite with minor amounts of dolomite, quartz, mica, and clay minerals. The minor phases can scarcely be distinguished on the diagrams because their reflections are either too feeble or overlapped and superposed by other more significant peaks. As it can be seen in Fig. 2, the K5 sample contains the highest amount of dolomite ($CaMg(CO_3)_2$), which is illustrated by small but visible reflections: main dolomite peak is located at 30.89°, and it is followed by two small reflections at 41.06° and 51°. This difference in the mineralogical composition of K5 limestone is in consistency with the chemical analysis (Tab. I), i.e. the K5 sample contained the highest percentage of MgO. In all investigated samples, the calcite was found to be the most abundant; therefore the most significant XRD reflections belong to this mineral phase. According to the chemical analysis, the calcium carbonate content varied from a low of 92.93 % for the K5 sample to a high of 99.09 % for the K19 sample. One of the main diversities between these two limestone samples is reflected in the intensities of their calcite

XRD peaks. Namely, the calcite peak of K19 limestone situated at 30° is approximately 300 arbitrary units higher than adequate peak of K5 sample. Also, the higher K19 crystallinity indicates presence of less amorphous solid. The K19 limestone has the highest calcite content, thusly it can be considered as a suitable resource for Portland cement manufacturing.

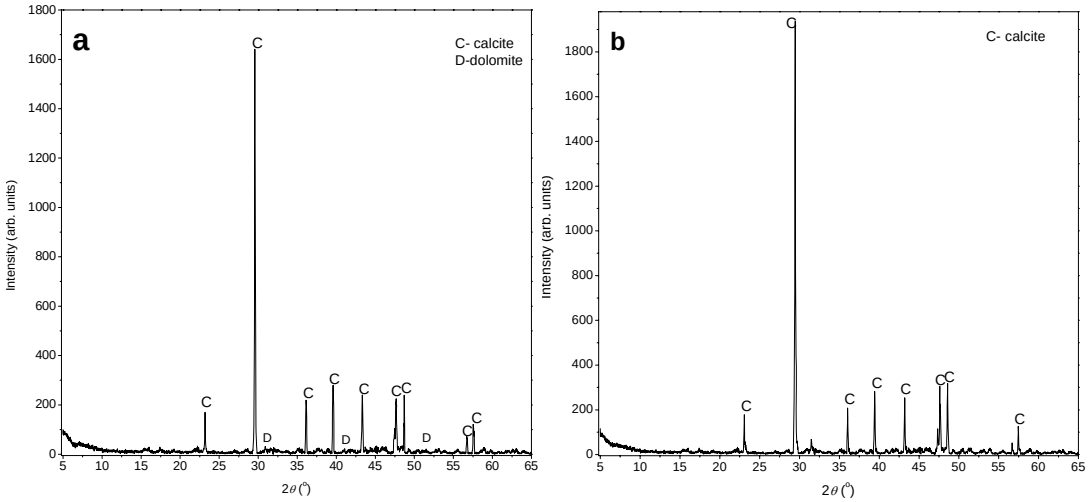

Fig. 2. XRD diffractogram of: a) K5 limestone sample; and b) K19 limestone sample.

Thermo-analytical methods are commonly applied in the investigations of mechanisms and kinetics of solid state decomposition reactions. The shape of a DTA and/or TG curve is a direct function of the kinetics of reactions that take place within material, and it is also interrelated with chemical and mineralogical characteristics of the limestone [39]. The limestone thermal behavior was assessed by means of the analysis of thermo-gravimetric and differential thermal curves of the samples that originated from 22 different deposits (K1-22). The testing has been conducted under same controlled atmosphere (described in Chapter 2.) The obtained results were afterwards compared and evaluated by PCA analysis. The DTA/TG diagrams of two representative samples (K5 and K19) are illustrated in Fig. 3a/b.

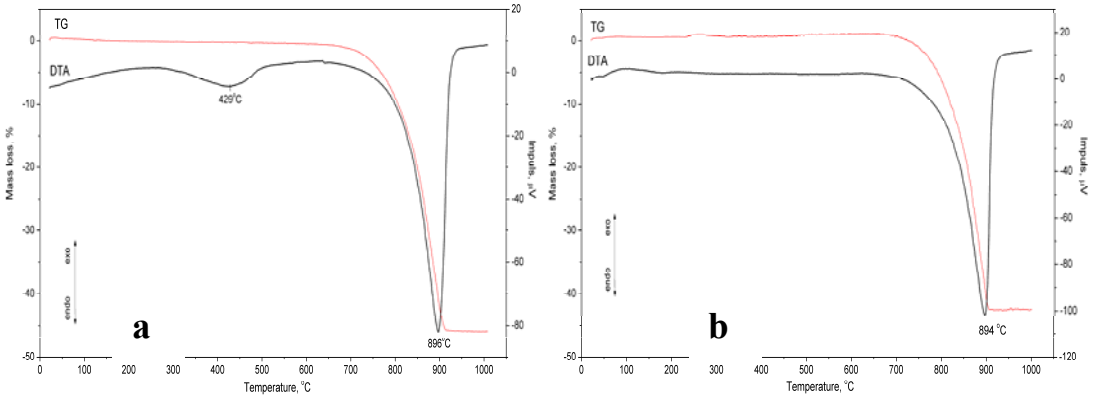

Fig. 3. DTA/TG curves of: a) K5 limestone; and b) K19 limestone.

The dominant thermally induced reaction that took place in the investigated limestone samples, which contained over 90 % of calcium carbonate, is calcination, i.e. decomposition of $CaCO_3$ induced by an exposure to strong heat. This reaction is important for the industrial application of limestone, primarily the cement production [2, 40]. In principle, $CaCO_3$ decomposes to lime (Eq. 1) if the ambient partial CO_2 pressure is below the equilibrium value of the partial pressure at a given temperature.

$$CaCO_3 \rightarrow CaO + CO_2 \quad (1)$$

Contrariwise, the formed lime is transformed back to carbonate if the partial CO_2 pressure exceeds this equilibrium value [2, 40]. The rate of the decomposition reaction is administered by the temperature of the reaction and heat transfer rate. When different limestone samples are subject to decomposition at high temperatures, a different behavior might be expected depending on the present impurities [21].

The calcination of the carbonate is an endothermic event; therefore a typical DTA curve for a sample of calcite rich limestone exhibits a single smooth decomposition step (Fig. 3a and b). High-calcium limestone decomposes at temperatures in the vicinity of 800-900 °C, in one stage with the formation of calcium oxide and carbon dioxide. The dissociation proceeds gradually from the outside surface inwards, with the reaction taking place at an interface between calcite and the residual oxide [2]. In contrast, the DTA curve for dolomite impure limestone (Fig. 3a) usually has two major endothermic peaks [40, 41]. The DTA curve of the K5 sample shows two peaks: the first, located at 429 °C, is associated with the formation of magnesia and calcite, and the second (at 896 °C) with the decomposition of calcite. The lower temperature DTA minimum, which commences at 350 °C and ends at 500 °C, is not distinct, it is rather wide endothermic hump that consists of numerous infinitesimal peaks. The shape of the higher temperature peak, which is related to the decomposition of the calcite, is exactly the same for both limestone samples with a small variation in final calcination temperature: 896 °C and 894 °C for K5 and K19, respectively. Immediately after this endothermic peak, DTA baseline does not drift neither endothermically nor exothermically, which means that there is no free lime present after the decomposition of calcite in the samples K5 and K19. The formation of the molten phase in the system did not appear in the applied thermal interval from 20° up to 1000 °C.

The TGA curves of the limestone samples K5 and K19 have an identical profile (Fig. 3a and b) showing only one peak of the mass variation due to completed thermal decomposition of the calcium carbonate. The major mass loss takes place at approximately 900 °C, and its values (measured in the temperature range from 650 °C to 900 °C) are 46.02 % and 44.43 % for K5 and K19, respectively. The values of the mass loss are in consistency with the obtained LoI. The slightly higher mass loss for the sample K5 is explained by later decomposition of the remaining dolomite mineral and impurities present in this sample.

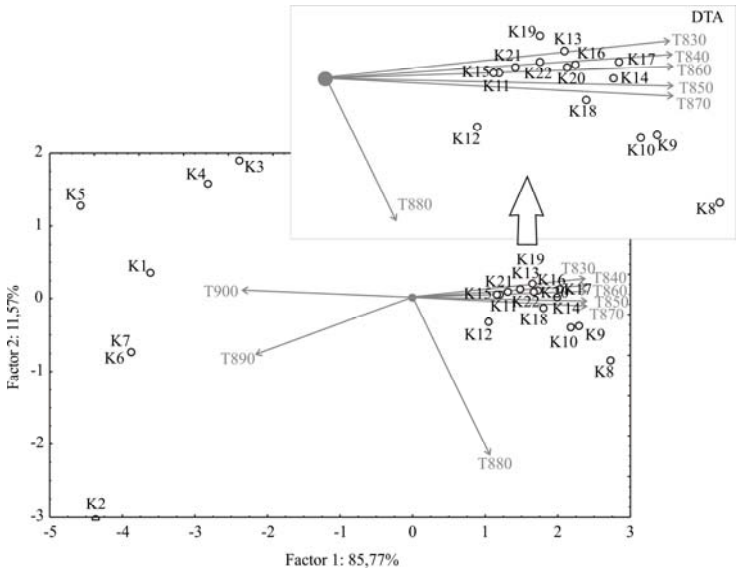

Fig. 4. Variables of limestone samples projection on the first factor plane, based on DTA peaks.

The analysis of the thermally induced dissimilarities in the limestone samples was conducted by means of the PCA. The DTA and TG output data acquired on the investigated samples K1-22 were statistically analyzed in proposed thermal interval from 650 to 900 °C (Fig. 4 and 5). The lower temperatures were not considered because only K5 sample exhibited DTA effects below 650 °C. The number of factors retained in the model, for proper classification of TGA data, in original matrix was observed as loading (different samples) and score (peak area) by application of Kaiser and Rice's rule. This criterion retained only principal components with Eigenvalues higher than 1.

In the DTA data registered on the diagram (Fig. 4), the first principal component (PC1) explained 85.77 % of the total variance, while the second principal component (PC2) was 11.57 %. The first Eigenvalue equals 6.86. The majority of DTA effects were observed in thermal interval from 830°-870 °C, and they were registered for the K8-22 samples. All manifested effects were endothermic. The minimal DTA peaks were exhibited in the analyses of the K3-5 samples. The maximal peaks were registered for the samples K1, K2, K6 and K7 in the thermal interval from 890°-900 °C.

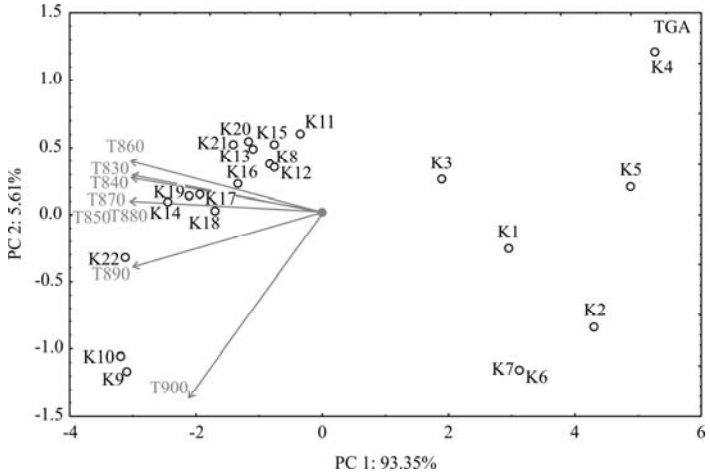

Fig. 5. Variables of limestone samples projection on the first factor plane, based on TG peaks.

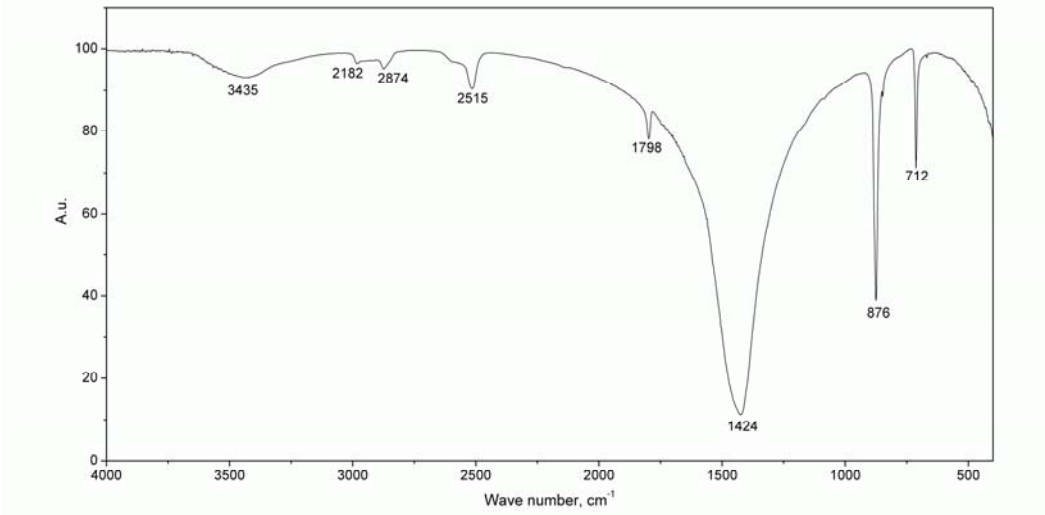

Fig. 6. FTIR spectra of the K19 limestone.

The first principal component (PC1) explained 93.35 % of the total variance (the first Eigenvalue equals 7.47), while the second principal component (PC2) was 5.61 % in the TGA data registered on the diagram (Fig. 5). The minimal changes in mass were observed for samples K1-K7, which is explained by lower content of $CaCO_3$. More significant thermally

induced changes in mass were observed for the samples K8, K11-13, K15-16 and K20-21, which comprised higher content of calcite mineral. The maximal weight changes were registered for the samples K9-10 and K22. Most of the samples underwent changes in the thermal interval from 830° to 880 °C, according to the PCA. Sample K19 is in the group of moderate mass loss which highlights its high calcite content and a small percentage of impurities in the composition.

Fourier Transform Infrared Spectroscopy (FTIR) was applied in the simultaneous qualitative analysis of calcite as the main calcium carbonate phase found in the twenty-two limestone samples (Fig. 6). The obtained FTIR spectra of the observed K1-22 samples were later studied and compared using the PCA statistical analysis (Fig.7).

The FTIR measurements were conducted in the wide region of 4000-400 cm^{-1}. The free carbonate ion belongs to the symmetry point group D_{3h}. Therefore, the CO_3^{2-} ion has four normal vibrations of which one belongs to the species A'_1, one is of species A'_2, while two vibrations belong to the E' species [42]. The carbonate functional group that is present in the calcite corresponds to the D_{3h} point group as a nonlinear with 4 atoms (N=4). This group has 3N-6=6 basic vibrations of which N-1=3 are valent [43]. The spectral difference between the more common groups may be related to crystal structure. The spectral relationships between the minerals of several groups are not well known, due to the complicated composition and crystal structure. Infrared active groups of CO_3, HCO_3, H_2O and OH normally dominate the absorption characteristics [43].

In the FTIR spectrum of the calcium carbonates ($CaCO_3$) the main absorption bands appear in the regions 1500-1400 cm^{-1}, 1100-1000 cm^{-1}, 900-800 cm^{-1} and close to 700 cm^{-1} [42]. The infrared spectra of the calcite and dolomite groups are normally characterized by three prominent absorption maxima and two minor peaks [43]. The analysis of the K19 sample showed eight peaks of different intensities on the diagram (given in Fig. 8): 3435, 2182, 2874, 2515, 1798, 1424, 876 and 712 cm^{-1}. The FTIR bands at 1424, 876 and 712 cm^{-1} had distinguished peaks, while the rest of the peaks were minor. The registered bands are all considered to be caused by the CO_3 groups with the crystals [43]. Namely, from the analysis of the space group characteristics, the existence of four molecular frequencies for the CO_3 ions in calcite is acknowledged of which three are active in the infrared spectrum [43-45].

Since the $CaCO_3$ contains less than one molecule of water per $CaCO_3$ in the structure [42], the bands that correspond to the three normal vibrations of the water molecule were found: at 3435, 2182, 2874 and 2515 cm^{-1} (anti-symmetric and symmetric O-H stretches), and at 1798 cm^{-1} (HOH bending). The band of medium intensity observed at 876 cm^{-1} is assigned to the V_2 which is a symmetric normal vibration of carbonate ion that corresponds to the CO_3 out-of-plane deformation mode. The strong, broad bond at 1424 cm^{-1} region corresponds to the symmetric normal V_3 vibration that is an asymmetric C-O stretching mode. A relatively weak absorption at 700 cm^{-1} can be related to the V_4 vibration which is characterized by in-plane deformation mode. As it can be seen in Fig. 6, the acknowledged bands are split and the band maxima is being observed at 1424, 876 and 712 cm^{-1}. Thereby, the site symmetry for CO_3^{2-} that is present in the limestone (i.e. calcite as the main phase) can be described as D_3 (A_1(R)(V_1), A_2(I)(V_2) and E(I,R)(V_3, V_4)) which is in agreement with the crystalline structure that can be determined via XRD measurements [42]. Also, a frequency value of the infrared inactive fundamental V_1 of calcite can be determined from the frequencies of two combination bands V_1+V_3 and V_1+V_4 observed at 2515 cm^{-1} and 1798 cm^{-1}, respectively, for the samples at low temperature, resulting in the average value 1088 cm^{-1} for V_1 which is in agreement with the value that can be obtained from the Raman spectra of calcite [44].

The investigation of the appropriate bands for the FTIR data analysis is a difficult task since there is a strong overlapping. Namely, the identified absorption bands that correspond to the similar wave number may have different peak intensities (Fig 7b). Therefore, the PCA analysis was performed on the FTIR spectra of the investigated limestone samples (Fig.7a).

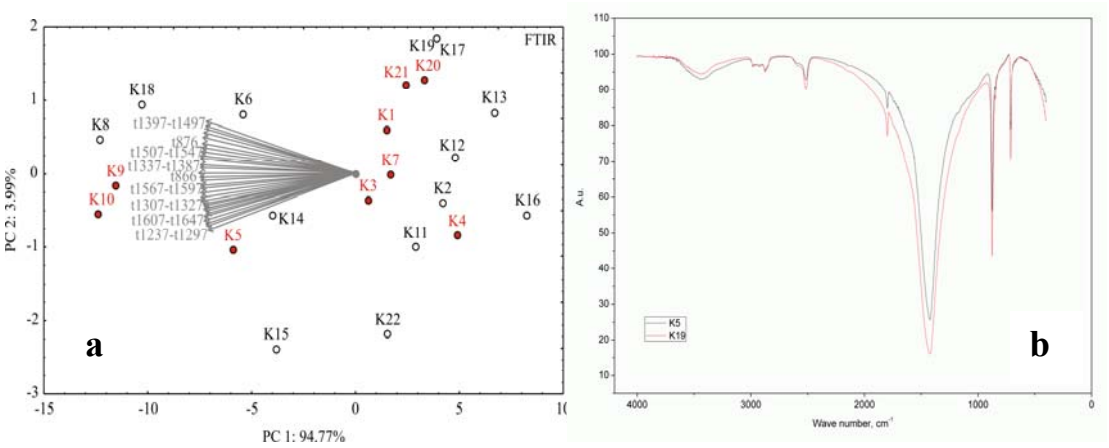

Fig. 7. Results of the FTIR analyses: a) variables of limestone samples projection on the first factor plane, based on FTIR spectra; and b) comparison of the K5 and K19 FTIR spectra.

The first principal component (PC1) in the analysis explained 94.77 % of the total variance. The first obtained Eigenvalue, in the data registered on the FTIR spectra, is equal to 42.65. The second principal component (PC2) in the FTIR data registered on the diagram was 3.99 %. The values of FTIR spectra exhibited the most profound diversities in the range 867-887 cm^{-1} and afterwards in 1237-1647 cm^{-1} where the two main absorption bands are located. The wave number of the third prominent peak, i.e. the band at 713 cm^{-1}, did not significantly varied in the observed twenty-two samples. These absorption bands located at approximately 1442, 877 and 713 cm^{-1} are characteristic for the $CaCO_3$. Thereby, these results confirm the conclusion of the XRD analysis that the samples mainly consisted of calcite mineral. The K19 sample had minimal variations from the theoretical calcite (714, 875 and 1473 cm^{-1} - the vibrations of the CO_3^{2-} that are characteristic for the $CaCO_3$) which indicates that K19 has the smallest impurities percentage in its composition.

The sample K19, which was selected as the limestone with the most appropriate composition for the production of construction composites was submitted to the scanning electron microphotography to acquire finer observations of the sample's microstructure (Fig. 8).

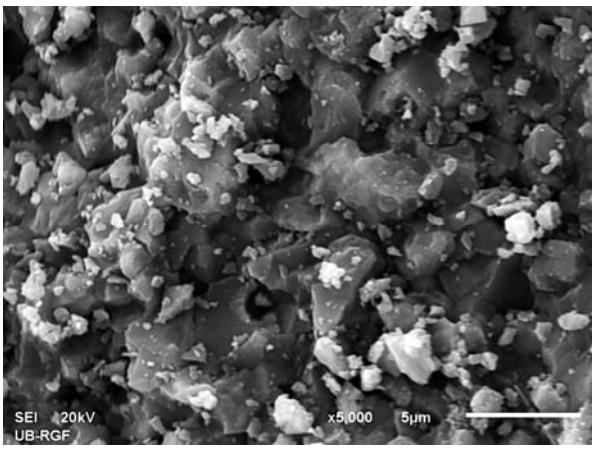

Fig. 8. SEM microphotograph of the K19 limestone.

The limestone usually comprises two types of particles: micrite which is a microcrystalline carbonate mud and sparite as sparry carbonate cement. Sparite is a coarser particle with the diameter varying from 20 to 100 μm in the original rock sample. Micrite,

which is of sedimentary origin, is formed of mechanically deposited calcareous particles ranging in diameter from 0.06 to 4 μm (in original rock sample). The majority of the rougher and clearly defined crystals correspond to the sparry calcite that fills interstitial pores as cement and represents either recrystallized micrite or a direct inorganic precipitate [46].

In the SEM microphotograph, presented in the Fig. 8, two types of the particles can be distinguished: larger crystals that might correspond to sparite and the calcite ooids which are probably formed of small calcareous crystals, i.e. micrite. Normally, micrite occurs as a matrix that fills or partly fills the interstitial pores between allochems [47, 48]. The limestone microstructure also comprises numerous small pores that are of nanometric and micrometric sizes. Coarse sparite crystals accompanied by ooids, located in between, are clearly identified by SEM. Both sparite and micrite are made of 100 % $CaCO_3$ [47, 48]. The differences in the crystal sizes of the limestone K19 is also visible. The variety in crystal sizes and the presence of porosity are important for the limestone that will be thermally processed [49]. Namely, a highly porous limestone possesses increased thermal resistance, because expansion/dilatation is likely to occur within the pores without causing significant damage to the surrounding structure [49]. Therefore, the investigated limestone samples are classified as a heterogeneous raw material that is not very sensitive to thermal changes. The K19 limestone is considered as structurally heterogeneous even though it is a mineralogically homogeneous material (i.e. it comprises only one mineral species - calcite). The reduced sensitivity to thermal treatment of the K19 limestone is a result of inter-particle porosity that enables distortion and/or rearrangement of the constituents without causing serious impact on the monocrystalline composition.

4. Conclusion

The limestone as an economically and environmentally sustainable resource that can have role of a cement replacement or mineral additive in a cementitious system was investigated. The study of the limestone chemistry and the thermal behavior proved to be crucial for the prognosis of construction composites properties. The instrumental methods' (AES, DTA/TG and FTIR) results were employed in the Principal component analysis to discriminate 22 limestone types and to choose the best output.

The PCA grouped the samples in a multi-dimensional factor space and produced four graphical prognoses - one per each instrumental analysis. The statistics of the chemical analysis indicated the K19 sample is the optimal limestone due to the high $CaCO_3$ content and low percentage of Fe_2O_3 and MgO. Thermal analyses and the PCA indicated that the majority of samples underwent changes in the thermal interval from 830° to 870/880 °C. Sample K19 had moderate mass loss due to the high calcite content and a small percentage of impurities in the composition. The FTIR spectra were the most diverse in two ranges: 867-887 cm^{-1} and 1237-1647 cm^{-1}. The obtained absorptions bands are characteristic for the $CaCO_3$, which confirmed the XRD analysis conclusion about calcite as the main mineral phase. The K19 sample had minimal variations from the theoretical calcite and it can be considered as structurally heterogeneous even though it is a mineralogically homogeneous. The reduced sensitivity to thermal treatment of the K19 limestone is a result of inter-particle porosity. Therefore the employing of powdery limestone in construction composites might produce properties comparable to that of conventional building materials.

This research confirmed that comparison of the samples using multivariate statistical techniques seems to be very efficient for the discrimination purposes, namely, it is possible to differentiate various limestone types and to predict the possibility of their employment in construction composites on the basis of the results of instrumental and mathematical analyses. Hence, the presented analysis of limestone showed the ability to differentiate between various samples and may have great potential as another method for authenticity control in practice.

Acknowledgements

This investigation was supported by Serbian Ministry of Education, Science and Technological Development and it was conducted under following projects: ON 172057, III 45008, TR 31055, TR 34006, and TR 34013.

5. References

1. S. Gunasekaran, G. Anbalagan, Spectrochimica Acta Part A, 69 (2008) 1246.
2. D. Dollimore, J. Dunn, Y. Lee, B. Penrod, Thermochimica Acta, 231 (1994) 125.
3. E. Yoğurtcuoğlu, M. Uçurum, Powder Technology, 214 (2011) 47.
4. K. De Weerdt, M. Haha, G. Saout, K. Kjellsen, H. Justnes, B. Lothenbach, Cement and Concrete Research, 41 (2011) 279.
5. I. Nafeaa, A. Zekry, M. Khalifa, A. Farag, N. El-Hussiny, M. Shalabi, Science of Sintering, 47 (2015) 319.
6. B. Felekoglu, Resources, Conservation and Recycling, 51 (2007) 770.
7. E. Anastasiou, A. Liapis, I. Papayianni, Resources, Conservation and Recycling, 101 (2015) 1.
8. P. Fabrykiewicz, I. Sosnowska, R. Przeniosło, Physica B, 496 (2016) 49.
9. R. McIntosh, J. Sharp, F. Wilburn, Thermochimica Acta, 165 (1990) 281.
10. U. Çavdar, E. Atik, A. Ataç, Science of Sintering, 46 (2014) 195.
11. L. M. Barcina, A. Espina, M. Sufirez, J. R. Garcia, J. Rodriguez, Thermochimica Acta, 290 (1997) 181.
12. Z. Zhang, Q. Wang, H. Chen, Powder Technology 301 (2016) 16.
13. P. Guzzo, J. Santos, R. David, International Journal of Mineral Processing, 126 (2014) 41.
14. A. Mahrous, M. Tantawi, H. El-Sageer, Construction and Building Materials, 24 (2010) 2598.
15. W. Cao, S. Liu, Z. Feng, Construction and Building Materials, 41 (2013) 474.
16. A. Elgalhud, R. Dhir, G. Ghataora, Cement and Concrete Composites, 72 (2016) 222.
17. G. Suaiam, N. Makul, Construction and Building Materials, 38 (2013) 455.
18. A. Arora, K. Vance, G. Sant, N. Neithalath, Construction and Building Materials, 121 (2016) 328.
19. M. Aqel, D. K. Panesar, Construction and Building Materials, 113 (2016) 359.
20. W. González-Gómez, P. Quintana, A. May-Pat, F. Avilés, J. May-Crespo, J. Alvarado-Gil, International Journal of Rock Mechanics & Mining Sciences, 75 (2015) 182.
21. F. Souza, S. Braganc, Thermochimica Acta, 561 (2013) 19.
22. J. W. Merks, Sampling and Sample Preparation at Mineral Processing Plants, (1986) 8. ISBN 0-87335-052-9
23. Lj. Andrić, A. Terzić, M. Petrov, J. Stojanović, M. Kostović, International Journal of Mineral Processing, 143 (2015) 1.
24. ASTM C25: Standard Test Methods for Chemical Analysis of Limestone, Quicklime, and Hydrated Lime.
25. ASTM C1271: Standard Test Method for X-Ray Spectrometric Analysis of Lime and Limestone.
26. ASTM C1301: Standard Test Method for Major and Trace Elements in Limestone and Lime by Inductively Coupled Plasma-Atomic Emission Spectroscopy (ICP) and Atomic Absorption (AA).
27. A. Covington, R. Bates, R. Durst, Pure Applied Chemistry, 57:3 (1985) 531.

28. H. Abdi, L. Williams, Principal component analysis, Wiley Interdisciplinary Reviews: Computational Statistics, 2:4 (2010) 433.
29. A. Terzić, L. Pezo, L. Andrić, Ceramic International, 41: 7 (2015) 8894.
30. A. Terzić, L. Pezo, L. Andrić, Composites B: Engineering, 79 (2015) 660.
31. www.statsoft.com (Data Analysis Software System 2010v10), Stat-Soft Inc., USA.
32. W. Klemm, L. Adams, Carbonate Additions to Cement, Publ. Philadelphia: ASTM (1990) pp. 60. ISBN: 0803114540 9780803114548
33. A. Ipavec, R. Gabrovšek, T. Vuk, K. Kaučič, J. Maček, A. Meden, Journal of the American Ceramic Society, 94 (2011) 1238.
34. M. Imbabi, C. Carrigan, S. McKenna, International Journal of Sustainable Built Environment, 1 (2012)194.
35. OECD/IEA and the World Business Council for Sustainable Development, Cement Technology Roadmap, 2009.
36. J. Schoon, A. Vergari, K. Buysser, I. Van Driessche, N. Belie, Construction and Building Materials, 43 (2013) 511.
37. F. Wali, K. Khan, W. Ali, F. Khan, 2nd International Conference on Energy, Environment & Sustainable Development (EESD2012), Pakistan (2012) 1.
38. M. Achternbosch, K. Brautigam, N. Hartlieb, C. Kupsch, U. Richers, P. Stemmerman, Heavy metals in cement and concrete resulting from the co-incineration of wastes in cement kilns with regard to the legitimacy of waste utilization, Forschungszentrum Karlsruhe GmbH, (2003) 15. ISSN 0947-8620
39. A. Mericboyu, S. Ktictikbayrak, R.Yavuz, Thermochimica Acta, 223 (1993) 121.
40. P. Anandakumaran, A. Bhattacharya, Thermochimica Acta, 59 (1982) 319.
41. Z. Tu, M. Guo, C.Poon, C. Shi, Cement and Concrete Composites, 72 (2016) 9.
42. F. Andersen, L. Brečević, Acta Chemica Scandinavica, 45 (1991) 1018.
43. C. K. Huang, P. F. Kerr, The American Mineralogist, 45 (1960) 311.
44. L. Hopkinson, K. Rutt, P. Kristova, J. Blows, C.Firth, Journal of Cultural Heritage, 16 (2015) 822.
45. N. Vagenas, A. Gatsouli, C. Kontoyannis, Talanta 59 (2003) 831.
46. https://www.britannica.com/science/sedimentary-rock
47. N. Mavropoulou, N. Katsiotis, J. Giannakopoulos, K. Koutsodontis, D. Papageorgiou, E. Chaniotakis, M. Katsioti, P. E. Tsakiridis, Construction and Building Materials, 124 (2016) 558.
48. M. Lion, F. Skoczylas, B. Ledesert, International Journal of Rock Mechanics & Mining Sciences, 42 (2005) 508.
49. F. Homand, J. P. Troalen, Engineering Geology, 20 (1984) 219.

Садржај: *Кречњак је, као економична и лако доступна сировина, често употребљиван у грађевинској индустрији у циљу разрешења проблема загађивања и заштите животне средине. Кречњак се најчешће инкорпорира у цементни систем млевењем заједно са цементним клинкером, или мешањем са везивом у поступку производње бетона. Применом прашкастих кречњака, као делимичне замене за цемент, добијају се конструкциони композити који поседују својства која су упоредива са својствима стандардних грађевинских бетона. Изучавање термичког понашања кречњака и његове хемије је од превасходне важности за предвиђање својстава пројектованих композита. У овом раду су употребљене инструменталне методе (атомска емисиона спектроскопија, диференцијално термијска и термогравиметријска анализа, и Фуријеова трансформациона инфрацрвена спектроскопија) и Метода главих компонената (PCA) у циљу препознавања и класификовања 22 различита типа кречњака. PCA статистичка метода, као средство идентификовања спектра и*

експерименталних резултата, груписала је узорке у мулти-димензиони факторни простор при томе формирајући четири графичке прогнозе – једну за сваку од инструменталних техника. Вредности DTA/TG пикова највише су варирали у кратком интервалу од 830° до 870 °C, док је FTIR спектар показао највише различитости у интервалима 867-887 и 1237-1647 cm^{-1}. Ово истраживање је руковођено идејом да се испита да ли је на основу комбинованих резултата инстументалних и математичких анализа могуће груписати различите типове кречњака и предвидети могућност њихове примене у констукционим композитима.

Кључне речи: *термичка својства; хемијска анализа; микроструктура; FTIR; DTA/TG; SEM; везиво; филер.*